Dalton Transactions

An international journal of inorganic chemistry

Accepted Manuscript

This article can be cited before page numbers have been issued, to do this please use: T. Thierry, V. Giuso, F. Polo, P. Mercandelli, Y. Chen, C. Chang, M. Mauro and S. Bellemin-Laponnaz, *Dalton Trans.*, 2024, DOI: 10.1039/D4DT00420E.

ROYAL SOCIETY OF CHEMISTRY

rsc.li/dalton

View Article Online
DOI: 10.1039/D4DT00420E

ARTICLE

A stable and true-blue emissive hexacoordinate Si(IV) N-heterocyclic carbene complex and its use in organic light-emitting diodes

Received 00th January 20xx,
Accepted 00th January 20xx

DOI: 10.1039/x0xx00000x

Thibault Thierry[ł a], Valerio Giuso[ł a], Federico Polo,[b,c] Pierluigi Mercandelli,[d] Yi-Ting Chen,[e] Chih-Hao Chang,[e] Matteo Mauro*[a] and Stéphane Bellemin-Laponnaz*[a]

A neutral hexacoordinate Si(IV) complex containing two tridentate N-heterocyclic carbene ligands is synthesised and characterized by X-ray crystallography, optical spectroscopy, electrochemistry and computational methods. The stable compound exhibits remarkable deep-blue photoluminescence particularly in the solid state that enables its use as electroluminescent material in organic light-emitting diodes.

Introduction

Organosilicon compounds are an interesting class of photo-functional species with appealing application as electroluminescent and electron transport materials as well as photodynamic therapy agents.[1] Selected examples are displayed in Chart 1. The majority of organosilicon derivatives are conjugated molecules that contain Si–C bond(s) and unique optoelectronic properties have been reported to date.[2–5] Hypercoordinated Si derivatives for such applications are much less explored. An interesting example is based on Si(IV) phthalocyanines where the tetracoordinated macrocycle helps stabilize otherwise labile Si-N bonds.[6] Little efforts have been devoted to the stabilization of silicon complexes using chelating bi- and/or tridentate architectures with C–Si, O–Si and N–Si bonds. Tetracoordinate N–Si complexes containing 1,2-*bis*(indol-2-yl)benzene have shown blue photoluminescence with high efficiency.[7] Dipyrromethene moieties have been used to form tetracoordinated Si complexes[8,9] and adjacent hydroxy anchors gave pentacoordinate O^N^N^O complexes with efficient red and near-IR luminescence.[10,11] More recently, hexacoordinate N–Si complexes featuring two 2,6-*bis*(benzimidazol-2-yl)pyridine *pincer*-type ligands have been prepared and displayed excellent optoelectronic properties and thermal stability have enabled their use in Organic Light-Emitting Diodes (OLEDs) and photovoltaic devices.[12,13] Silicon remains very attractive as a tetravalent, earth-abundant, non-toxic lightweight atom and it often has significant influence on the optical and electronic properties. On the other hand, there is currently a great interest in developing stable deep-blue emitters for light-emitting devices. Despite these promising recent examples, the coordination chemistry of Si(IV) chelates is still overlooked most likely due to its supposed instability.

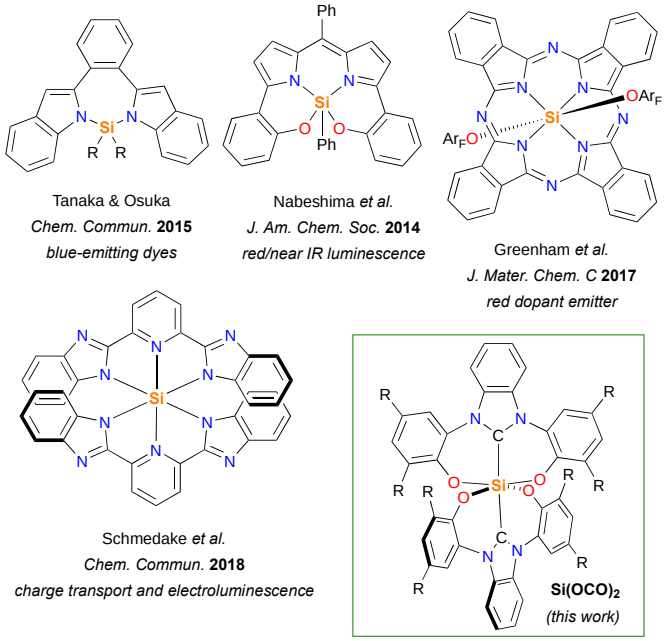

Chart 1. Selected examples of tetra-, penta- and hexacoordinate Si complexes with remarkable photophysical properties and molecular structure of the **Si(OCO)$_2$** complex.

N-heterocyclic carbenes (NHCs) have been recognised as a privileged ligands in organometallic chemistry of transition metals,[15–17] and to provide robust (electro)luminescent materials for optoelectronics.[18,19] Interestingly, the use of NHC to stabilize Si(IV) is gaining increasing attention.[14] Although these latter can stabilize low valence states and induce new

[a] Institut de Physique et Chimie des Matériaux de Strasbourg UMR 7504 - Université de Strasbourg & CNRS, 23 rue du Loess, 67034 Strasbourg, France
Email: bellemin@unistra.fr; mauro@unistra.fr
[b] Department of Molecular Sciences and Nanosystems, Ca' Foscari University of Venice, Via Torino 155, 30172 Venice, Italy.
[c] European Centre for Living Technology (ECLT), Ca' Foscari University of Venice, Ca' Bottacin, 30124, Venice, Italy.
[d] Università degli Studi di Milano, Dipartimento di Chimica, 20133 Milan, Italy.
[e] Department of Electrical Engineering, Yuan Ze University, 32003 Taoyuan, Taiwan.
ł T.T. and V.G. have equally contributed to this work.

Electronic Supplementary Information (ESI) available: General experimental remarks, details including the synthesis, X-ray crystallographic data, ^{1}H, ^{13}C{^{1}H} ^{19}F{^{1}H} NMR spectra, additional photophysical, electrochemical, and computational characterisation as well as OLED device fabrication. CCDC 2284375 (compound **Si(OCO)$_2$**).

reactivities,[20–24] they have been mostly used with halogenated Si(IV) reagents to exploit its hypervalent pentacoordinate Si(IV) intermediates and, more recently, to stabilize less common Si(IV) alkoxysilanes with highly electronegative *bis*-trifluoroalkoxy ligands. Pentacoordinate NHC–Si intermediates have been postulated to account for the stability of free NHC carbenes in silicones as well.[25]

A few years ago we introduced a new family of LX_2 *pincer*-type NHC ligands with O^C^O motif, namely **(OCO)H$_3$**, characterised by a central imidazolylidene NHC moiety with two lateral chelating phenolic groups (see Scheme 1).[26,27] This ligand has proven to be very versatile and robust for coordinating oxophilic metals with high oxidation state such as Ti(IV), Zr(IV) and Hf(IV).[28–32] Herein, we report the synthesis and comprehensive characterization of a homoleptic, neutral, hexacoordinate luminescent complex, namely **Si(OCO)$_2$**, that displays high thermal and photo-stability in solution and in solid state under air and moisture. The optical properties are investigated and elucidated also by the help of computational approaches. Finally, proof-of-concept OLED devices are successfully fabricated, and the electroluminescent performances described.

Results and discussion

The complex **Si(OCO)**$_2$ was straightforwardly synthesized from $SiCl_4$ and the corresponding benzimidazolium precursor **(OCO)H$_3$** resulting in a robust and air stable compound that can be easily purified by column chromatography (Scheme 1 and ESI for experimental details).[33] NMR data are reported in Figure S1–S3 of the ESI. ^{1}H NMR spectrum displays a highly symmetric resonance pattern consistent with an average D_{2d} symmetry of the molecule, expectedly, as shown in Figure S1 in the ESI. ^{29}Si NMR spectroscopy confirms the hexacoordinate nature of the silicon with a $\delta = -197.4$ ppm (Figure S3), a chemical shift in the same range as the hexacoordinated complex reported by Schmedake and coworkers that display a $\delta = -186$ ppm (see Chart 1).[12]

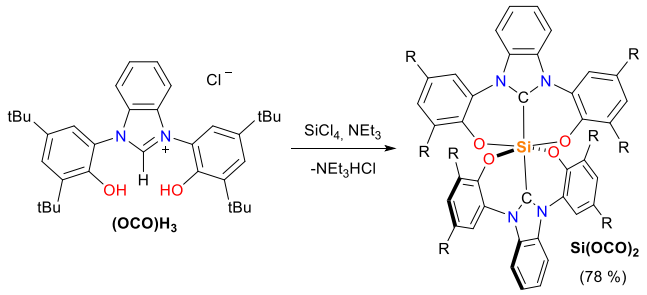

Scheme 1. Synthetic pathway used for the preparation of complex **Si(OCO)$_2$**.

Single crystals suitable for X-ray investigation were obtained and the structure is displayed in Figure 1 and S4. Crystallographic refinement parameters are listed in Table S1 of the ESI. In the crystal structure, the silicon center adopts an octahedral geometry with C_{NHC} atoms located mutually in *trans* geometry. The Si–O distances are long with average bond length *d*(Si–O) = 1.78 Å, typical for a hypervalent silicon and the *d*(Si–C_{NHC}) = 1.90 Å. The phenolates are outside the plane formed by the carbene heterocycle with an average angle of *ca.* 41° between the two phenolate planes of the ligand, with an O–Si–O angle of 174.7°. Interestingly, the **Si(OCO)$_2$** complex displays a very high thermal stability as demonstrated by thermogravimetric analysis where degradation starts above 200°C with 5% weight loss temperature $T_{5\%}$ as high as 352°C (Figure S5). Cyclic voltammetry was employed to assess the electrochemical behavior of **Si(OCO)$_2$** in CH_2Cl_2 solution. At negative potentials it is present an irreversible reduction process R_1 at –2.30 V vs Fc|Fc$^+$, which is assigned to the reduction of the ligand (see Fig. S6 and Table S2 in the ESI).

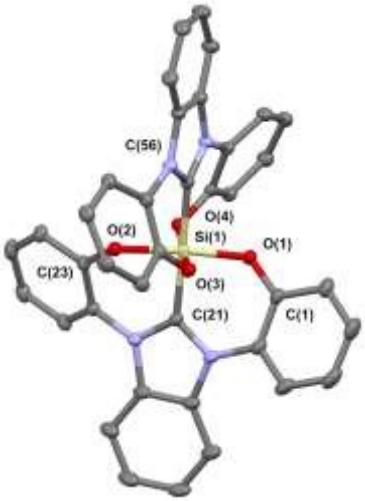

Figure 1. Molecular structure of **Si(OCO)$_2$** (CCDC 2284375). The tBu groups and H atoms are omitted for clarity. Selected bond lengths [Å] and angles [°]: Si(1)-O(1), 1.7707(15); Si(1)-O(4), 1.7709(15); Si(1)-O(3), 1.7849(15); Si(1)-O(2), 1.7865(15); Si(1)-C(56), 1.904(2); Si(1)-C(21) 1.909(2); O(1)-Si(1)-O(4), 89.80(7); O(1)-Si(1)-O(3), 89.67(7); O(4)-Si(1)-O(3), 174.50(7); O(1)-Si(1)-O(2), 174.84(7).

Density functional theory (DFT) computations were performed on a species analogous to **Si(OCO)$_2$** in which the *tert*-butyl substituents on the phenyl rings have been replaced by methyl groups, namely **Si(O^{Me}CO^{Me})$_2$**. The optimized geometry of the latter complex in its ground state shows an exact S_4 symmetry. Molecular orbitals (MOs) closer to the frontier region and displayed in Figure 2, whereas a larger set of MOs density surfaces is reported in Figure S9, together with their symmetry and energy.

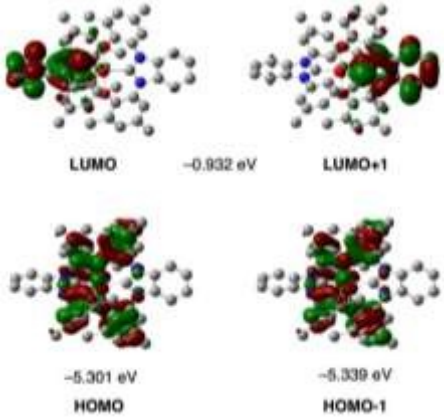

View Article Online
DOI: 10.1039/D4DT00490E

Figure 2. MOs isodensity surfaces of HOMO–1 to LUMO+1 computed for compound **Si(O^{Me}CO^{Me})$_2$.**

The eight higher-energy filled orbitals are located on the four phenolate moieties. They are various combination (of a, b and e symmetry) of the *p* orbitals of the oxygen atoms with two of the π orbitals of the phenyl groups (corresponding to the e_{1g} degenerate bonding orbitals of benzene). The first four lower unoccupied molecular orbitals are located on the two NHC moieties. The degenerated LUMOs of e symmetry have contribution mainly from the five-membered rings while the next two orbitals (of a and b symmetry) mainly from the six-membered rings. The following two degenerated orbitals are somehow delocalized all over the molecule. No significant contribution from the silicon atom can be found in any of the orbitals described.

The experimental electronic absorption and emission spectra recorded for **Si(OCO)$_2$** and the comparison with the pro-ligand **(OCO)H$_3$** are displayed in Figure 3 and data are summarized in Table 1. For dilute CH_2Cl_2 samples (2×10^{-5} M), the UV-Vis spectrum of **Si(OCO)$_2$** displays three main regions of absorption with broad profile. The two bands at lower energy, λ_{abs} = 332 and 299 nm display lower intensity, with $\varepsilon = 1.3\times10^4$ and 1.5×10^4 M^{-1} cm^{-1} respectively. A more intense band is present with maximum at λ_{abs} = 271 nm ($\varepsilon = 2.2\times10^4$ M^{-1} cm^{-1}).

Table 1. Photophysical properties of **Si(OCO)$_2$** and **(OCO)H$_3$** in dilute air-equilibrated CH_2Cl_2 solution (2.0×10^{-5} M) at room temperature, in 2-MeTHF glassy matrix at 77 K and in the solid state as crystalline powders. Radiative and non-radiative rate constants were determined with the equations $k_r = PLQY/\tau$ and $k_{nr} = (1 - PLQY)/\tau$ respectively. *sh* denotes a shoulder.

	λ_{max} (ε) [nm, (10^3 M^{-1} cm^{-1})]	λ_{em} [nm]	PLQY (%)	τ_{obs} [ns]	$\bar{\tau}_{obs}$ [ns]	k_r [10^7 s^{-1}]	k_{nr} [10^8 s^{-1}]	λ_{em} [nm]	PLQY (%)	τ_{obs} [ns]	$\bar{\tau}_{obs}$ [ns]	k_r [10^7 s^{-1}]	k_{nr} [10^7 s^{-1}]	λ_{em} [nm]	τ_{obs} [ns]	$\bar{\tau}_{obs}$ [ns]
	CH_2Cl_2, 2×10^{-5} M, air-equilibrated							*crystalline solid*						*77 K, 2-MeTHF*		
(OCO)H$_3$	274 (12.25), 280 (12.01)	485	1	1.87	-	0.5	5.3	434	1	5.7 (38%) 1.81 (62%)	4.38	0.23	22.6	410, 436, 467, 500*sh*	1.75 (34%) 1.11 (64%)	1.58
Si(OCO)$_2$	271 (21.55), 299*sh* (15.02), 332 (12.88)	437, 456*sh*	2	0.21	-	9.6	46.9	418	32	2.98	-	10.7	22.8	414, 433, 462*sh*	1.35 (25%) 5.60 (75%)	4.31

Time-dependent DFT (TD-DFT) supported the photophysical characterization. Given the composition of the HOMOs and LUMOs, all the transitions up to *ca.* 4.95 eV (corresponding to ca. 250 nm) are mainly intraligand charge transfer (^{1}ILCT) transitions, characterized by a large electron density displacement (ca. 0.25–0.45 *e*$^-$) from the phenolate moieties to the NHC rings. In particular, the transitions computed at 348 nm (S_1 and S_2, of E symmetry), 309 nm (S_8), and 280 nm (S_{12}) involve both the NCN atoms and the annulated ring of the NHC moiety, while the transitions computed at 283 nm (S_9 and S_{10}, of E symmetry) and 274 nm (S_{13} and S_{14}, of E symmetry) involve the six-membered ring only. All the degenerate transitions correspond to transfer of electrons within a single ligand with $\pi_{OPh}\rightarrow\pi^*_{NHC}$ nature. In addition, transitions S_9, S_{10} and S_{12} involve excitations in orbitals delocalized also on the OPh groups, assuming a partial $\pi_{OPh}\rightarrow\pi^*_{OPh}$ character. Data for all the described transitions is reported in Table S3.

In the experimental absorption of pro-ligand **(OCO)H$_3$** only the band at λ_{abs} = *ca.* 270 nm is present with about half of the intensity compared to that observed for **Si(OCO)$_2$**, supporting these attributions. Additionally, a more intense ($\varepsilon = 5.5\times10^4$ M^{-1} cm^{-1}) band is clearly visible at λ_{abs} = 245 nm in solvents of larger optical transparency window (e.g. THF) that can be ascribed with confidence to singlet-manifold $^1\pi\rightarrow\pi^*$ processes mainly involving the NHC scaffold (Figure S7). Minor solvent effect is observed for the lower energy band at λ_{abs} = *ca.* 340 nm that shifts bathochromically by *ca.* 440 cm^{-1} upon decreasing solvent polarity in the series MeOH → CH_2Cl_2 → THF → toluene. Despite the overall CT character of the transitions, small solvatochromism is observed since these excitation processes involve both the O_{PhO}^C_{NHC}^O_{PhO} chromophoric scaffolds with an overall spherically symmetric redistribution of the electron-hole pair density at Franck-Condon.

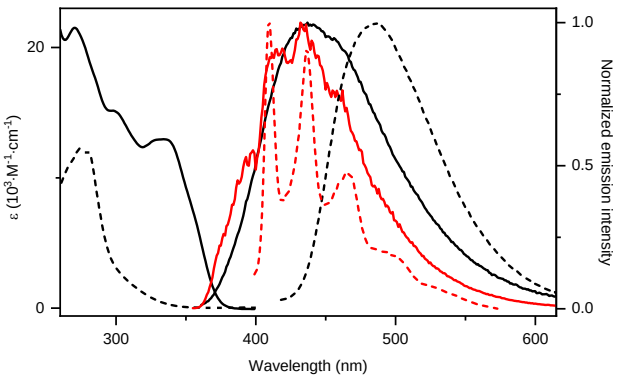

Figure 3. UV-vis absorption and photoluminescence emission in dilute CH_2Cl_2 (2×10^{-5} M) (black traces) and in 2-MeTHF glassy matrix at 77 K (red traces) for complex **Si(OCO)$_2$** (solid traces) and pro-ligand **(OCO)H$_3$** (dashed traces). Emission spectra were recorded upon excitation at λ_{exc} = 320 and 360 nm for **Si(OCO)$_2$** and **(OCO)H$_3$**, respectively.

Upon photoexcitation in the lower-energy band, samples of **Si(OCO)$_2$** in CH_2Cl_2 display deep-blue emission with broad and structureless profile peaking at λ_{em} = 437 nm with photoluminescence quantum yield (PLQY) of 2% (Figure 3 and Table 1). This emission arises from a short-lived excited state τ = 209 ps, insensitive to oxygen quenching. The high radiative rate constant (k_r) for this process ($k_r = 9.6\times10^7$ s^{-1}) is characteristic of a strongly allowed transition originating from a

View Article Online
DOI: 10.1039/D4DT00430F

singlet manifold. On the other hand, the non-radiative rate constant (k_{nr}) was as high as $4.9.6\times10^9$ s^{-1}, indicative of the presence of efficient quenching channels coupling with the emitting excited state. The quenching is attributable to the rotational motion of the *tert*-butyl substituents, the fluxional twisting motion of the two PhO–Si–OPh moieties and the large geometrical distortion occurring in the S_1 (Table S3). The emission $S_1 \rightarrow S_0$ is computed at 481 / 394 nm (vertical / adiabatic). The large difference between the S_0 and S_1 geometries is responsible for the significant difference between the two computed values. The corresponding electron density-difference map shows the expected electron transfer from the NHC moiety to the OPh groups (ca. 0.40 e^-, see Figure 4).

Emission spectra appear to be slightly influenced by the solvent with an overall shift by about 926 cm^{-1} from MeOH to CH_2Cl_2 (Figure S7). An increase of the PLQY up to 4% is also observed in MeOH and toluene samples along with a prolongation of the excited state lifetime (Table S3). Solvent polarity is likely not the only parameter affecting the emission solvatochromism of this compound: specific solvent-solute interactions are expected to be at play as well. As a consequence, being based on a polarizable continuum model, TD-DFT results only qualitatively agree with the observed shift due to solvent effects (Table S6).

Photophysical measures of **Si(OCO)$_2$** carried out in 2-MeTHF glassy matrix at 77 K yield a slightly structured emission profile with minor hypsochromic shift compared to the emission in fluid THF and a few ns-scale lifetime, indicative of a partial ^{1}CT character. On the other hand, for **(OCO)H$_3$** the spectrum at 77 K becomes highly structured and shows larger hypsochromic shift, supporting the sizeable ^{1}CT character of the excited state in the cationic pro-ligand (see Figure 3).

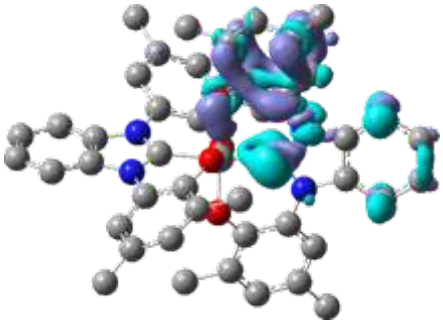

Figure 4. Electronic density-difference map computed (at the optimized S_1 geometry) for the vertical transition $S_1 \rightarrow S_0$ of the methyl-substituted analogue of **Si(OCO)$_2$**. Cyan and violet colour indicates a decrease and increase in electron density, respectively.

Table 2. Photophysical properties of **Si(OCO)$_2$** spin-coated thin films.

compound	doping % polymer	λ_{em} [nm]	PLQY (%)	CIE (x, y)	τ_{obs} [ns]	$\bar{\tau}_{obs}$ [ns]
Si(OCO)$_2$	10% PMMA 120k	419	28	0.17, 0.11	1.75 (30%) 4.43 (62%)	4.01
	10% PS 35k	420	32	0.17, 0.11	2.94 (64%) 5.08 (36%)	3.98

Remarkably, spin-coated thin film samples of **Si(OCO)$_2$** at 10 wt.% doping level in polymer matrices such as poly-methylmetacrylate (PMMA) and polystyrene (PS) switch-on the emission properties of the samples as consequence of the rigidification of the environment and restriction of the roto-vibrational freedom of the emitters. Indeed, doped thin films display intense, structureless, deep-blue photoluminescence with maximum at λ_{em} = 419 and 422 nm, and PLQY as high as 28% and 32%, respectively (Figure S8 and Table 2) with CIE_y coordinate as low as 0.11, making **Si(OCO)$_2$** of great potential interest for the fabrication of deep-blue OLED devices. Interestingly, crystalline samples of **Si(OCO)$_2$** show a narrower emission profile at λ_{em} = 418 nm due to the even more rigid environment provided by the dense crystal packing with PLQY of 32%. The **(OCO)H$_3$** derivative, on the other hand, shows low (PLQY = 1%) and red-shifted emission at λ_{em} = 434 nm in the solid state. For both species, this emission is ascribed to an excited state with ^{1}ILCT ($^1\pi_{PhO} \rightarrow \pi^*_{NHC}$, $S_1 \rightarrow S_0$) character.

Owing its interesting photophysical properties, the **Si(OCO)$_2$** complex was employed as emitter in vacuum-processed OLED devices to explore its potential as electroluminescent material under various doping concentration between 8 and 20 wt.%. The device performances in terms of electroluminescence (EL) spectra, current density–voltage–luminescence (*J*-*V*-*L*), external quantum efficiency vs luminance and luminance efficiency vs luminance are displayed in Figure 5. The corresponding details and additional characteristics of the fabricated OLEDs are provided in Figure S10 and Table S7 of the ESI. The optimized architecture for the tested devices was as follows ITO (120 nm)/TAPC:MoO_3 20 wt.% (5 nm)/TAPC (25 nm)/TCTA (10 nm)/ mCP:**Si(OCO)$_2$** (20 nm)/TmPyPB (50 nm)/LiF (0.8 nm)/Al (120 nm), where TAPC is 1,1-bis[(di-4-tolylamino)phenyl]cyclohexane, TCTA is 4,4',4"-tris(carbazol-9-yl)-triphenylamine, mCP is N,N'-dicarbazolyl-3,5-benzene and TmPyPB is 1,3,5-tri[(3-pyridyl)-phen-3-yl]benzene (TmPyPB).

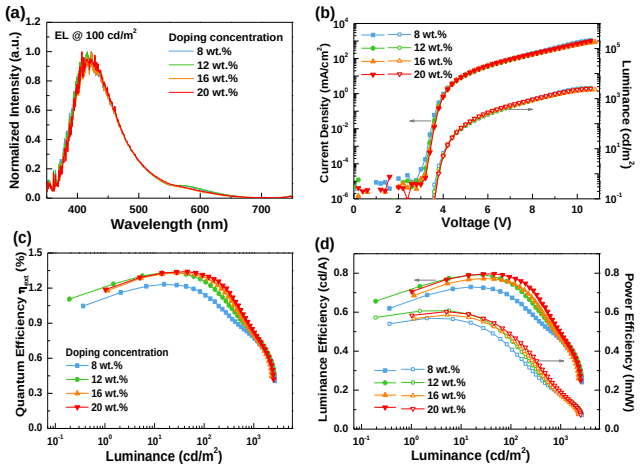

Figure 5. Normalized EL spectra at a luminance of 100 cd m^{-2}; (b) current density–voltage–luminance (*J*–*V*–*L*) characteristics of OLED devices with different doping concentrations; (c) external quantum efficiency vs luminance; (d) luminance/power efficiency vs luminance for the devices with different doping concentrations.

The OLED devices fabricated embedding complex **Si(OCO)$_2$** in the electroluminescent layer showed featureless and relatively narrow EL spectra peaking at $\lambda_{EL,max}$ = 408–423 nm depending on the doping concentration in the investigated range. The EL spectra largely resembled the profile observed in the photoluminescence measurements of doped thin films at 10 wt.% doping level in either PMMA or PS polymer matrix (see above). This is indicative of the fact that the same excited state is involved in both photo- and electro-generated luminescence process. Optimized devices displayed adequate EL performance with peak external quantum efficiency (EQE) of 1.3% (0.8 cd A^{-1}), maximum luminance value of 2566 cd m^{-2} and saturated true-blue emission. Notably, the tested devices with varying doping concentration showed similar EL performances, including the current density, luminance, efficiency, and spectrum, highlighting **Si(OCO)$_2$** is insensitive to doping level.

Conclusions

In conclusion, we have synthesized and characterized a neutral hexacoordinate Si(IV) complex containing two tridentate N-heterocyclic carbene ligands. Our studies included X-ray crystallography, optical spectroscopy, electrochemistry and computational methods. The homoleptic complex exhibits remarkable dark-blue photoluminescence, particularly in the solid state, enabling it to be used as an electroluminescent material in organic light-emitting diodes. This study demonstrates the benefits of combining silicon and carbenes for achieving a novel class of stable emitters based on the Si(IV)-NHC core and suitable as true-blue EL materials in OLED devices for the first time.

Experimental details

General experimental remarks and details including the synthesis, the X-ray crystallographic analysis, NMR spectroscopy, photophysical, electrochemical, and computational characterisation as well as OLED device fabrication can be found in the ESI section along with the additional data.

Acknowledgements

This work was supported by the Université de Strasbourg and the CNRS. This research was financed in part by the French National Research Agency (Agence Nationale de la Recherche - ANR) under the project ANR-22-CE07-0049-01, the ITI-CSC via the IdEx Unistra (ANR-10-IDEX-0002), and the National Science and Technology Council (Taiwan) under the project " NSTC 112-2923-E-155-002-MY4. N. Kyritsakas of the Service de Radiocristallographie, Fédération de chimie Le Bel – FR2010, Université de Strasbourg & CNRS is kindly acknowledged for the help in solving the X-ray structure.

Conflicts of interest

There are no conflicts to declare.

Notes and references

View Article Online
DOI: 10.1039/D4DT00420E

1 N. Auner and J. Weis, *Organosilicon Chemistry III From Molecules to Materials*, Wiley-VCH, Weinheim 2008.
2 Y. Tokoro, H. Yeo, K. Tanaka and Y. Chujo, *Chem. Commun.*, 2012, **48**, 8541.
3 S. Yamaguchi and K. Tamao, *J. Chem. Soc., Dalton Trans.*, 1998, 3693–3702.
4 K. L. Chan, M. J. McKiernan, C. R. Towns and A. B. Holmes, *J. Am. Chem. Soc.*, 2005, **127**, 7662–7663.
5 J. Luo, Z. Xie, J. W. Y. Lam, L. Cheng, B. Z. Tang, H. Chen, C. Qiu, H. S. Kwok, X. Zhan, Y. Liu and D. Zhu, *Chem. Commun.*, 2001, 1740–1741.
6 A. J. Pearson, T. Plint, S. T. E. Jones, B. H. Lessard, D. Credgington, T. P. Bender and N. C. Greenham, *J. Mater. Chem. C*, 2017, **5**, 12688–12698.
7 T. Tanaka and A. Osuka, *Chem. Commun.*, 2015, **51**, 8123–8125.
8 A. Kämpfe, E. Kroke and J. Wagler, *Organometallics*, 2014, **33**, 112–120.
9 A. Kämpfe, E. Brendler, E. Kroke and J. Wagler, *Chem. Eur. J.*, 2014, **20**, 9409–9418.
10 N. Sakamoto, C. Ikeda, M. Yamamura and T. Nabeshima, *J. Am. Chem. Soc.*, 2011, **133**, 4726–4729.
11 M. Yamamura, M. Albrecht, M. Albrecht, Y. Nishimura, T. Arai and T. Nabeshima, *Inorg. Chem.*, 2014, **53**, 1355–1360.
12 M. Kocherga, J. Castaneda, M. G. Walter, Y. Zhang, N.-A. Saleh, L. Wang, D. S. Jones, J. Merkert, B. Donovan-Merkert, Y. Li, T. Hofmann and T. A. Schmedake, *Chem. Commun.*, 2018, **54**, 14073–14076.
13 M. Kocherga, K. M. Boyle, J. Merkert, T. A. Schmedake and M. G. Walter, *Mater. Adv.*, 2022, **3**, 2373–2379.
14 V. Nesterov, D. Reiter, P. Bag, P. Frisch, R. Holzner, A. Porzelt and S. Inoue, *Chem. Rev.*, 2018, **118**, 9678–9842.
15 M. N. Hopkinson, C. Richter, M. Schedler and F. Glorius, *Nature*, 2014, **510**, 485–496.
16 C. Romain, S. Bellemin-Laponnaz and S. Dagorne, *Coord. Chem. Rev.*, 2020, **422**, 213411.
17 S. Bellemin-Laponnaz and S. Dagorne, *Chem. Rev.*, 2014, **114**, 8747–8774.
18 Y. Chi, T.-K. Chang, P. Ganesan and P. Rajakannu, *Coord. Chem. Rev.*, 2017, **346**, 91–100.
19 A. Bonfiglio and M. Mauro, *Eur. J. Inorg. Chem.*, 2020, 3427–3442.
20 D. Lutters, C. Severin, M. Schmidtmann and T. Müller, *J. Am. Chem. Soc.*, 2016, **138**, 6061–6067.
21 Y. Wang, M. Chen, Y. Xie, P. Wei, H. F. Schaefer, P. von R. Schleyer and G. H. Robinson, *Nature Chem.*, 2015, **7**, 509–513.
22 Y. Xiong, S. Yao, R. Müller, M. Kaupp and M. Driess, *Nature Chem.*, 2010, **2**, 577–580.
23 Y. Wang, M. Chen, Y. Xie, P. Wei, H. F. Schaefer and G. H. Robinson, *J. Am. Chem. Soc.*, 2015, **137**, 8396–8399.
24 A. Burchert, S. Yao, R. Müller, C. Schattenberg, Y. Xiong, M. Kaupp and M. Driess, *Angew. Chem. Int. Ed.*, 2017, **56**, 1894.
25 F. Bonnette, T. Kato, M. Destarac, G. Mignani, F. P. Cossío and A. Baceiredo, *Angew. Chem. Int. Ed.*, 2007, **46**, 8632–8635.
26 S. Bellemin-Laponnaz, R. Welter, L. Brelot and S. Dagorne, *J. Organomet. Chem.*, 2009, **694**, 604–606.
27 S. Bellemin-Laponnaz, S. Dagorne, R. Dümpelmann and P. Steffanut, *Chimia*, 2014, **68**, 500.
28 C. Romain, B. Heinrich, S. B. Laponnaz and S. Dagorne, *Chem. Commun.*, 2012, **48**, 2213.

View Article Online
DOI: 10.1039/D4DT00420E

29 S. Dagorne, S. Bellemin-Laponnaz and C. Romain, *Organometallics*, 2013, **32**, 2736–2743.
30 C. Romain, C. Fliedel, S. Bellemin-Laponnaz and S. Dagorne, *Organometallics*, 2014, **33**, 5730–5739.
31 E. Borré, G. Dahm, A. Aliprandi, M. Mauro, S. Dagorne and S. Bellemin-Laponnaz, *Organometallics*, 2014, **33**, 4374–4384.
32 C. Romain, S. Choua, J.-P. Collin, M. Heinrich, C. Bailly, L. Karmazin-Brelot, S. Bellemin-Laponnaz and S. Dagorne, *Inorg. Chem.*, 2014, **53**, 7371–7376.
33 L. Benhamou, E. Chardon, G. Lavigne, S. Bellemin-Laponnaz and V. César, *Chem. Rev.*, 2011, **111**, 2705–2733.